Synthesis and Characterization of Seven-Coordinate Tantalum(I) and Niobium(I) Complexes with Cis Carbonyl and Alkyl Isocyanide Ligands

Edmund M. Carnahan, R. Lynn Rardin, Simon G. Bott, and Stephen J. Lippard*

Department of Chemistry, Massachusetts Institute of Technology, Cambridge, Massachusetts 02139

Received June 4, 1992

A series of seven-coordinate tantalum(I) and niobium(I) complexes of the form $[M(CNR)(CO)(dmpe)_2Cl]$ [M = Nb, R = Me, Cy, Bu^t; M = Ta, R = Me, Et, Bu^t; dmpe = 1,2-bis(dimethylphosphino)ethane] has been synthesized by photolysis of $[M(CO)_2(dmpe)_2Cl]$ in the presence of CNR. The bis(isocyanide) complex $[Ta(CNMe)_2(dmpe)_2Cl]$ was prepared by reduction of $[TaCl_4(dmpe)_2]$ in the presence of CNMe. These extremely electron-rich compounds are fluxional in solution, displaying low-temperature NMR spectra consistent with a capped trigonal prismatic or pentagonal bipyramidal geometry. Single-crystal X-ray analyses of four of these compounds revealed extensively bent C–N–C isocyanide linkages. The isocyanide bend angles for $[Ta(CNMe)_2(dmpe)_2Cl]$ are close to 120°, suggesting that the ligands are bound to the metal as heteroallenes. The suitability of the niobium(I) and tantalum(I) compounds as precursors for reductive coupling of CO and CNR ligands is discussed. Crystal data: $[Nb(CNCy)(CO)(dmpe)_2Cl]$, monoclinic, $P2_1/c$, a = 18.900 (3) Å, b = 9.180 (1) Å, c = 16.627 (2) Å, β = 95.417 (6)°, Z = 4, R = 0.038, R_w = 0.042; $[Ta(CNEt)(CO)(dmpe)_2Cl]$, monoclinic, $P2_1/n$, a = 9.082 (4) Å, b = 30.453 (7) Å, c = 9.214 (4) Å, β = 105.75 (2)°, Z = 4, R = 0.031, R_w = 0.042; $[Ta(CNBu^t)(CO)(dmpe)_2Cl]$, monoclinic, $P2_1/n$, a = 9.399 (2) Å, b = 32.188 (6) Å, c = 9.406 (5) Å, β = 103.03 (3)°, Z = 4, R = 0.042, R_w = 0.052; $[Ta(CNMe)_2(dmpe)_2Cl]$, triclinic, $P\bar{1}$, a = 17.389 (1) Å, b = 17.467 (3) Å, c = 9.111 (2) Å, α = 99.99 (2)°, β = 94.75 (1)°, γ = 110.89 (1)°, Z = 4, R = 0.034, R_w = 0.047.

Introduction

Our interest in low-valent, seven-coordinate early transition metal complexes stems from the discovery that two adjacent carbonyl[1,2] or alkyl isocyanide[3-6] ligands in such species can be reductively coupled to afford functionalized acetylene ligands, eqs 1–3. Recent mechanistic studies of these coupling reactions[7-11]

$$[M(CO)_2(dmpe)_2X] \xrightarrow[Na/Hg]{40\%} \xrightarrow{Me_3SiX} [M(Me_3SiOC{\equiv}COSiMe_3)(dmpe)_2X] \quad (1)$$

M = Nb, Ta; X = Cl

$$[M(CNR)_6X]^+ \xrightarrow[\text{trace } H_2O]{Zn,\ THF} [M(RHNC{\equiv}CNHR)(CNR)_4X]^+ \quad (2)$$

M = Mo, W; R = alkyl

X = halide, CN^-

$$[Mo(CNR)_5(bpy)]^{2+} \xrightarrow[\text{trace } H_2O]{Zn,\ THF} [Mo(RHNC{\equiv}CNHR)(CNR)_3(bpy)]^{2+} \quad (3)$$

R = Bu^t

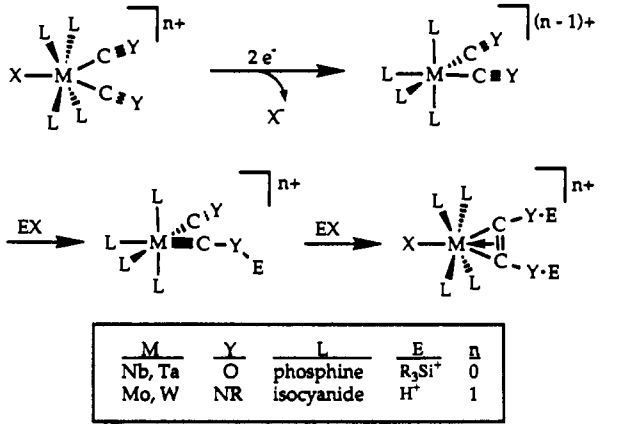

M	Y	L	E	n
Nb, Ta	O	phosphine	R_3Si^+	0
Mo, W	NR	isocyanide	H^+	1

Figure 1. Schematic representation of the mechanism for the reductive coupling of two carbonyl or alkyl isocyanide ligands.

revealed that they follow a common mechanistic pathway (Figure 1). Reduction of the seven-coordinate d^4 starting complex with loss of halide generates a six-coordinate, d^6 intermediate. These electron-rich species are susceptible to electrophilic attack at the heteroatom of an isocyanide or carbonyl ligand to form heteroatom-substituted carbyne species. Addition of a second equivalent of EX induces CO- or CNR–carbyne coupling to form the final metal-bound acetylene complex (Figure 1). The coupling of two carbonyl ligands in a related vanadium complex proceeds analogously, although the product does not contain a capping ligand when X is triflate.[12]

Having shown that the mechanisms for C≡O and C≡NR coupling reactions were analogous, we wished to see whether both ligand coupling reactions could occur within the same metal

(1) Bianconi, P. A.; Vrtis, R. N.; Rao, C. P.; Williams, I. D.; Engeler, M. P.; Lippard, S. J. *Organometallics* **1987**, *6*, 1968.
(2) Bianconi, P. A.; Williams, I. D.; Engeler, M. P.; Lippard, S. J. *J. Am. Chem. Soc.* **1986**, *108*, 311.
(3) Warner, S.; Lippard, S. J. *Organometallics* **1986**, *5*, 1716.
(4) Giandomenico, C. M.; Lam, C. T.; Lippard, S. J. *J. Am. Chem. Soc.* **1982**, *104*, 1263.
(5) Dewan, J. C.; Giandomenico, C. M.; Lippard, S. J. *Inorg. Chem.* **1981**, *20*, 4069.
(6) Lam, C. T.; Corfield, P. W. R.; Lippard, S. J. *J. Am. Chem. Soc.* **1977**, *99*, 617.
(7) Vrtis, R. N.; Liu, S.; Rao, C. P.; Bott, S. G.; Lippard, S. J. *Organometallics* **1991**, *10*, 275.
(8) Vrtis, R. N.; Lippard, S. J. *Isr. J. Chem.* **1990**, *30*, 331.
(9) Vrtis, R. N.; Rao, C. P.; Warner, S.; Lippard, S. J. *J. Am. Chem. Soc.* **1988**, *110*, 2669.
(10) Carnahan, E. M.; Lippard, S. J. *J. Chem. Soc., Dalton Trans.* **1991**, 699.
(11) Filippou, A. C.; Grünleitner, W. *J. Organomet. Chem.* **1990**, *393*, C10.
(12) Protasiewicz, J. D.; Lippard, S. J. *J. Am. Chem. Soc.* **1991**, *113*, 6564.

0020-1669/92/1331-5193$03.00/0

framework. In addition, we sought suitable precursor molecules to effect the cross coupling of C≡O with C≡NR. Apart from increasing the scope of the reductive coupling reaction, cross coupling would generate the previously unknown (ROC≡CNR'R'') ligand. The successful coupling of carbonyl ligands in $[M(CO)_2(dmpe)_2Cl]$ complexes (eq 1) led us to choose as target starting materials low-valent alkyl isocyanide species, $[M(CNR)_{2-n}(CO)_n(dmpe)_2Cl]$ (M = Nb, Ta; dmpe = 1,2-bis(dimethylphosphino)ethane; n = 0, 1). Reaction chemistry following the general pattern shown in Figure 1 would result in the desired ligand couplings for these complexes.

There are relatively few isocyanide complexes of the group V metals when compared to those of group VI and later transition metals.[13] In part, this difference is caused by the interesting insertion and coupling reactions exhibited by many early transition metal isocyanides (see below). A number of vanadium and niobium isocyanide complexes containing one or two cyclopentadienyl ligands are known.[14-19] The vanadium adducts $[VCl_3(CNR)_3]$,[20] $[V(CNR)_6]^+$,[20] $[V(CNBu^t)_2(dmpe)_2](PF_6)_2$,[21] $[VCl_3(CNBu^t)(\equiv NPh)]_2$, and $[VCl_3(CNBu^t)_2(\equiv NPh)]$[22] have been prepared, as have the highly-reduced $[M(CO)_5(CNR)]^-$ anions (M = V, Nb, Ta).[23-25] Depending upon reaction conditions, addition of RNC to $[Nb_2Cl_6(SMe_2)_3]$ afforded either the $[Nb_3Cl_8(CNR)_5]$ clusters[26] or $[NbCl_2(CNR)_4(\mu^2\text{-}\eta^4\text{-}RNCCNR)\text{-}NbCl_4]$,[27,28] in which two isocyanide ligands have been coupled. Addition of RNC to group V metal compounds containing metal–alkyl bonds often leads to formation of η^2-iminoacyl complexes,[29] which can react further with another iminoacyl[30,31] or a bound acetylene[32] to give insertion products.

Previously, we reported that seven-coordinate carbonyl and alkyl isocyanide tantalum(I) and niobium(I) complexes can be reductively coupled.[33,34] In the present article we describe full details of the synthesis and characterization of the mixed isocyanide–carbonyl complexes, $[M(CNR)(CO)(dmpe)_2Cl]$. Single-crystal X-ray structures are reported for four of these compounds, and their physical and spectroscopic properties are discussed. One member of this class, $[Nb(CNBu^t)(CO)(dmpe)_2Cl]$, previously described by us,[33] was independently obtained while the present work was in progress.[35] Attempts to find alternative synthetic pathways to these complexes resulted in the formation of $[Ta(CNMe)_2(dmpe)_2Cl]$, which also can be reductively coupled.[34] The synthesis and characterization of this bis(isocyanide) complex, which contains extensively bent MeNC ligands, are also reported.

Experimental Section

General Considerations. Tetrahydrofuran (THF), dimethoxyethane (DME), diethyl ether, and pentane were distilled from sodium benzophenone ketyl under nitrogen. $[Ta(CO)_2(dmpe)_2Cl]$,[36,37] $[Nb(CO)_2(dmpe)_2Cl]$,[36,38] $[TaCl_4(dmpe)_2]$,[37,39] methyl isocyanide (MeNC),[40] and ethyl isocyanide (EtNC)[40] were prepared by literature methods. *tert*-Butyl isocyanide (Bu^tNC) and cyclohexyl isocyanide (CyNC) were purchased from commercial vendors and used without further purification. All experiments were carried out either in a nitrogen-filled Vacuum Atmospheres drybox or with the use of conventional Schlenk line techniques under purified argon. Photolyses were performed by using a 450-W mercury Hanovia lamp filtered through Pyrex. Infrared spectra were recorded on Mattson Cygnus 100 or Bio-Rad FTS7 Fourier transform instruments. NMR spectra were obtained by using Varian XL-300 or VXR-500 spectrometers. ^1H NMR spectra were referenced to residual solvent protons and ^{31}P NMR spectra to an external sample of 85% H_3PO_4. Elemental analyses were performed by Analytische Laboratorien GMBH, Engelskirchen, Germany, and Oneida Research Services, Inc., Whitesboro, NY.

$[Nb(CNMe)(CO)(dmpe)_2Cl]$ (1). A solution of 0.147 g (0.303 mmol) of $[Nb(CO)_2(dmpe)_2Cl]$ and 0.140 mL (3.78 mmol) of CNMe in 20 mL of THF was divided into two flasks and photolyzed for 15 min, causing a color change from yellow-orange to dark red-brown. The solvent was removed in vacuo and the solid extracted with 5 mL of pentane. Filtration of the cherry red solution and removal of solvent yielded **1** (0.076 g, 50.3% based on Nb) as a red, microcrystalline solid. The brown residue from the reaction was redissolved in 10 mL of THF and was passed through a 2-in. pad of silica to recover 0.061 g (41.5%) of pure starting material, $[Nb(CO)_2(dmpe)_2Cl]$, which was recycled to make more **1**. The product could be further purified by recrystallization from pentane at −30 °C with a reduction in yield. FTIR (KBr): 2967 (m), 2901 (m), 2850 (w), 1830 (s), 1752 (s), 1420 (m), 1391 (m), 1245 (m), 1279 (m), 1140 (w), 1100 (w), 940 (s), 930 (s), 888 (m), 727 (m), 700 (m), 641 (m) cm^{-1}. ^1H NMR (298 K, 300 MHz, C_6D_6): δ 3.18 (s, $CNCH_3$), 1.39 (br, PCH_3), 1.02 ppm (br, PCH_2). Anal. Calcd for $C_{15}H_{35}NOP_4ClNb$ (**1**): C, 36.20; H, 7.09; N, 2.81; P, 24.89. Found: C, 36.23; H, 7.18; N, 2.74; P, 24.90.

$[Nb(CNBu^t)(CO)(dmpe)_2Cl]$ (2). A solution of 0.217 g (0.448 mmol) of $[Nb(CO)_2(dmpe)_2Cl]$ and 0.200 mL (3.27 mmol) of $CNBu^t$ in 20 mL of THF was photolyzed for 45 min as described above for **1**. The solvent was stripped and the cherry-red product extracted into 10 mL of pentane. Removal of solvent yielded bright red microcrystals of $[Nb(CNBu^t)(CO)(dmpe)_2Cl]$ (0.157 g, 65.0% based on Nb). The product was recrystallized from pentane at −30 °C to yield large red blocks of **2** (0.122 g, 50.5%). FTIR (KBr): 2966 (w), 2899 (m), 1879 (s), 1751 (s), 1718 (w), 1419 (m), 1275 (w), 938 (s), 927 (m), 910 (m), 889 (m), 725 (w), 695 (m), 638 (m) cm^{-1}. ^1H NMR (293 K, 300 MHz, C_6D_6): 1.7–1.55 (br, PCH_2), 1.43 (br, PCH_3), 1.36 (NBu^t) ppm. Anal. Calcd for $C_{18}H_{41}ClNONbP_4$ (**2**): C, 40.05; H, 7.66; N, 2.59; P, 22.95. Found: C, 40.25; H, 7.28; N, 2.65; P, 23.65.

$[Nb(CNCy)(CO)(dmpe)_2Cl]$ (3). A solution of 0.153 g (0.316 mmol) of $[Nb(CO)_2(dmpe)_2Cl]$ and 0.140 mL (1.47 mmol) of CyNC in 20 mL of THF was photolyzed for 15 min as described above for **1**. The solvent was removed and the resulting red oil extracted into pentane. Cooling of a concentrated pentane solution to −30 °C yielded **3** as large red plates (0.052 g, 29.2% based on Nb). FTIR (KBr): 2923 (m), 2903 (m), 2853 (w), 1782 (s), 1724 (s), 1420 (w), 1294 (w), 1124 (w), 940 (m), 930 (m),

(13) Crociani, B. In *Reactions of Coordinated Ligands*; Braterman, P. S., Ed.; Plenum Press: New York, 1986; Vol. 1, p 553.
(14) Gómez, M.; Ilarduya, J. M. M. d.; Royo, P. *J. Organomet. Chem.* **1989**, *369*, 197.
(15) Burger, B. J.; Santarsiero, B. D.; Trimmer, M. S.; Bercaw, J. E. *J. Am. Chem. Soc.* **1988**, *110*, 3134.
(16) Ilarduya, J. M. M. d.; Otero, A.; Royo, P. *J. Organomet. Chem.* **1988**, *340*, 187.
(17) Coville, N. J.; Harris, G. W.; Rehder, D. *J. Organomet. Chem.* **1985**, *293*, 365.
(18) Fachinetti, G.; Nero, S. D.; Floriani, C. *J. Chem. Soc., Dalton Trans.* **1976**, 1046.
(19) Fachinetti, G.; Floriani, C. *J. Chem. Soc., Chem. Commun.* **1975**, 578.
(20) Silverman, L. D.; Dewan, J. C.; Giandomenico, C. M.; Lippard, S. J. *Inorg. Chem.* **1980**, *19*, 3379.
(21) Anderson, S. J.; Wells, F. J.; Wilkinson, G. *Polyhedron* **1988**, *7*, 2615.
(22) Carofiglio, T.; Floriani, C.; Chiesi-Villa, A.; Guastini, C. *Inorg. Chem.* **1989**, *28*, 4417.
(23) Warnock, G. F. P.; Sprague, J.; Fjare, K. L.; Ellis, J. E. *J. Am. Chem. Soc.* **1983**, *105*, 672.
(24) Ellis, J. E.; Fjare, K. L. *Organometallics* **1982**, *1*, 898.
(25) Ellis, J. E.; Fjare, K. L. *J. Organomet. Chem.* **1981**, *214*, C33.
(26) Cotton, F. A.; Roth, W. J. *Inorg. Chim. Acta* **1987**, *126*, 161.
(27) Cotton, F. A.; Duraj, S. A.; Roth, W. J. *J. Am. Chem. Soc.* **1984**, *106*, 6987.
(28) Cotton, F. A.; Roth, W. J. *J. Am. Chem. Soc.* **1983**, *105*, 3734.
(29) Durfee, L. D.; Rothwell, I. P. *Chem. Rev.* **1988**, *88*, 1059.
(30) Chamberlain, L. R.; Steffey, B. D.; Rothwell, I. P.; Hoffman, J. C. *Polyhedron* **1989**, *8*, 341.
(31) Chamberlain, L. R.; Durfee, L. D.; Fanwick, P. E.; Kobriger, L. M.; Latesky, S. L.; McMullen, A. K.; Steffey, B. D.; Rothwell, I. P.; Folting, K.; Huffman, J. C. *J. Am. Chem. Soc.* **1987**, *109*, 6068.
(32) Curtis, M. D.; Real, J.; Hirpo, W.; Butler, W. M. *Organometallics* **1990**, *9*, 66.
(33) Carnahan, E. M.; Lippard, S. J. *J. Am. Chem. Soc.* **1990**, *112*, 3230.
(34) Carnahan, E. M.; Lippard, S. J. *J. Am. Chem. Soc.* **1992**, *114*, 4166.
(35) Aharonian, G.; Hubert-Pfalzgraf, L. G.; Zaki, A.; Le Borgne, G. *Inorg. Chem.* **1991**, *30*, 3105.
(36) Protasiewicz, J. D.; Bianconi, P. A.; Williams, I. D.; Liu, S.; Rao, Ch. P.; Lippard, S. J. *Inorg. Chem.* **1992**, *31*, 4134.
(37) Datta, S.; Wreford, S. S. *Inorg. Chem.* **1977**, *16*, 1134.
(38) Burt, R. J.; Leigh, G. J.; Hughes, D. L. *J. Chem. Soc., Dalton Trans.* **1981**, 793.
(39) Leutkens, M. L., Jr.; Elcesser, W. L.; Huffman, J. C.; Sattelberger, A. P. *Inorg. Chem.* **1984**, *23*, 1718.
(40) Casanova, J.; Schuster, R. E.; Werner, N. D. *J. Chem. Soc.* **1963**, 4280.

Table I. X-ray Crystal Structure Data Collection Parameters[a] for [Nb(CNCy)(CO)(dmpe)$_2$Cl] (**3**), [Ta(CNEt)(CO)(dmpe)$_2$Cl] (**5**), [Ta(CNBu^t)(CO)(dmpe)$_2$Cl] (**6**), and [Ta(CNMe)$_2$(dmpe)$_2$Cl] (**7**)

	3	**5**	**6**	**7**
a (Å)	18.900 (3)	9.082 (4)	9.399 (2)	17.389 (1)
b (Å)	9.180 (1)	30.453 (7)	32.188 (6)	17.467 (3)
c (Å)	16.627 (2)	9.214 (4)	9.406 (5)	9.111 (2)
α (deg)				99.99 (2)
β (deg)	95.417 (6)	105.75 (2)	103.03 (3)	94.75 (1)
γ (deg)				110.89 (1)
V (Å^3)	2872.1 (6)	2452 (1)	2772 (3)	2514.4 (8)
temp (°C)	−70	−50	+23	−78
fw	565.82	599.77	627.82	598.79
Z	4	4	4	4
ρ_{calc} (g cm^{-3})	1.31	1.63	1.50	1.58
space group	$P2_1/c$	$P2_1/n$	$P2_1/n$	$P\bar{1}$
angle limits (deg)	$2 \le 2\theta \le 50$	$3 \le 2\theta \le 50$	$2 \le 2\theta \le 50$	$3 \le 2\theta \le 50$
data limits	$+h,+k,\pm l$	$+h,+k,\pm l$	$+h,+k,\pm l$	$+h,\pm k,\pm l$
μ (cm^{-1})	7.25	48.03	42.51	46.77
no. of total data	5686	4678	6536	9551
no. of unique data	5384	4393	4969	8845
R(merge)[b]	2.4	4.9	4.6	2.8
no. of unique observed[c] data	2852	2994	2919	6592
no. of LS params	253	217	235	433
p factor	0.05	0.05	0.05	0.05
R[d]	0.038	0.031	0.042	0.034
R_w	0.042	0.042	0.052	0.047

[a] Data collected on an Enraf-Nonius CAD-4F κ geometry diffractometer using Mo K$\bar{\alpha}$ radiation. [b] R(merge) = $\sum_{i=1}^{n}\sum_{j=1}^{m}|\langle F_i^2\rangle - F_{ij}^2|/\sum_{i=1}^{n} m \times \langle F_i^2\rangle$ where n = number unique reflections observed more than once, m = number of times a given reflection was observed, and $\langle F_i^2\rangle$ is the average value of F^2 for reflection i. [c] Observation criterion $I > 3\sigma(I)$. [d] $R = \sum||F_o| - |F_c||/\sum|F_o|$, $R_w = [\sum w(|F_o| - |F_c|)^2/\sum w|F_o|^2]^{1/2}$, where $w = 1/\sigma^2(F)$ and $\sigma(F)$ is defined in eq 7.

892 (m), 729 (w), 701 (w), 642 (w) cm^{-1}. ^{1}H NMR (293 K, 300 MHz, C_6D_6): 3.80 (m, 1 H, NC*H*), 2.00 (m, 2 H, C–CH_2), 1.58 (m, 4 H, C–CH_2), 1.43 (24 H, PCH_3), 1.10 (m, 4 H, C–CH_2) ppm. The dmpe methylene resonances were not resolved from the other broad resonances. Anal. Calcd for $C_{20}H_{43}ClNNbOP_4$: C, 42.46; H, 7.66; N, 2.48. Found: C, 43.10; H, 7.06; N, 2.92.

[Ta(CNMe)(CO)(dmpe)$_2$Cl] (4). A solution of 0.210 g (0.367 mmol) of [Ta(CO)$_2$(dmpe)$_2$Cl] and 0.160 mL (4.43 mmol) of CNMe in 20 mL of THF was photolyzed for 30 min. Workup and recovery of [Ta(CO)$_2$(dmpe)$_2$Cl] as described above and repeat of the reaction yielded **4** (0.110 g, 51.2% based on Ta) as a red, microcrystalline solid. FTIR (KBr): 2968 (w), 2902 (s), 2856 (w), 1809 (s, br), 1746 (s, br), 1419 (m), 1390 (m), 1295 (w), 1278 (m), 938 (s), 888 (m), 727 (m), 700 (m), 641 (m) cm^{-1}. ^{1}H NMR (291 K, 300 MHz, toluene-d_8): 3.26 (NCH_3), 1.6–1.3 (br, PCH_3), 1.1–0.8 (br, PCH_2) ppm. ^{31}P{^{1}H} NMR (213 K, 202.3 MHz, THF-d_8): 28.16 (d, J_{P-P} = 42 Hz), 22.42 (d, J_{P-P} = 42 Hz) ppm. Anal. Calcd for $C_{15}H_{35}ClNOP_4Ta$ (**4**): C, 30.76; H, 6.02; N, 2.39. Found: C, 30.82; H, 5.93; N, 2.07.

[Ta(CNEt)(CO)(dmpe)$_2$Cl] (5). A 30-min photolysis of 0.201 g (0.351 mmol) of [Ta(CO)$_2$(dmpe)$_2$Cl] and 0.100 mL (1.33 mmol) of CNEt in 20 mL of THF yielded 0.095 g (45.1% based on Ta) of **5** following workup as described above for **1**. The crude product was recrystallized from pentane at −30 °C to yield large red plates of **5** (0.055 g, 26.1%). FTIR (KBr): 2968 (w), 2904 (m), 2861 (w), 1776 (s), 1722 (s), 1417 (m), 1326 (m), 1283 (m), 1236 (w), 1125 (w), 1081 (w), 1016 (w), 938 (s), 893 (m), 837 (m), 728 (m), 699 (m), 642 (m), 589 (w) cm^{-1}. ^{1}H NMR (293 K, 300 MHz, C_6D_6): 3.56 (q, J_{C-H} = 7.2 Hz, 2 H, NCH_2), 1.7–1.4 (br, PCH_2), 1.40 (br, PCH_3), 1.15 (t, J_{C-H} = 7.2 Hz, 3 H, CCH_3) ppm. ^{31}P{^{1}H} NMR (236 K, 121 MHz, THF-d_8): 26.85 (d, J_{P-P} = 83 Hz), 22.70 (d, J_{P-P} = 85 Hz) ppm. Anal. Calcd for $C_{16}H_{37}ClNOP_4Ta$ (**5**): C, 32.04; H, 6.22; N, 2.34. Found: C, 31.69; H, 6.48; N, 2.25.

[Ta(CNBu^t)(CO)(dmpe)$_2$Cl] (6). A 45-min photolysis of 0.204 g (0.356 mmol) of [Ta(CO)$_2$(dmpe)$_2$Cl] and 0.200 mL (3.27 mmol) of CNBu^t in 20 mL of THF yielded 0.096 g (42.9% based on Ta) of **6** upon workup as described above for **1**. An additional 0.097 g (47.5%) of the starting [Ta(CO)$_2$(dmpe)$_2$Cl] complex was recovered. Characterization of **6**: FTIR (KBr) 2967 (m), 2902 (m), 1808 (s), 1747 (s), 1419 (m), 1358 (w), 1278 (w), 1234 (w), 1194 (w), 940 (s), 891 (m), 678 (w), 640 (w) cm^{-1}. The band at 1747 cm^{-1} shifts to 1705 cm^{-1} when starting with [Ta(^{13}CO)$_2$(dmpe)$_2$Cl]. ^{1}H NMR (293 K, 300 MHz, C_6D_6) 1.51 (br, PCH_3), 1.41 (br, PCH_3), 1.38 (sh, NB*u^t*) ppm; the methylene resonances were not resolved; ^{31}P{^{1}H} NMR (198 K, 202.3 MHz, THF-d_8): 24.50 (d, J_{P-P} = 70 Hz), 22.31 (d, J_{P-P} = 70 Hz) ppm. Anal. Calcd for $C_{18}H_{41}ClNOP_4Ta$ (**6**): C, 34.44; H, 6.58; N, 2.23. Found: C, 34.35; H, 6.45; N, 2.97.

[Ta(CNMe)$_2$(dmpe)$_2$Cl] (7). To a solution of 0.310 g (0.498 mmol) of [TaCl$_4$(dmpe)$_2$] in 15 mL of THF were added 3 equiv of 0.5% Na/Hg and 2 equiv (41 μL, 1.09 mmol) of CNMe. The blue solution slowly turned dark burgundy over a 24-h period, after which the solution was filtered and the solvent removed in vacuo. The residue was extracted with two 10-mL portions of pentane. The combined extracts were filtered, and the solvent was removed. The red, sticky solid was extracted into ~5 mL of pentane, carefully leaving behind as much of the yellow [TaCl$_2$(dmpe)$_2$] impurity as possible. Cooling of the pentane solution to −30 °C yielded **7** as large plates (0.097 g, 32.6%). Characterization of **7**: FTIR (KBr) 2966 (w), 2899 (s), 2849 (w), 1737 (s), 1695 (s), 1416 (m), 1373 (s), 1287 (w), 1279 (w), 923 (s), 892 (m), 641 (m), 593 (m) cm^{-1}; ^{1}H NMR (239 K, 300 MHz, C_6D_6) 3.07 (t, NCH_3, J_{N-H} = 1.5 Hz), 1.47 (br, PCH_3) ppm; the dmpe methylene resonances were not resolved; ^{31}P{^{1}H} NMR (293 K, 121 MHz, C_6D_6) 27.29 ppm. Anal. Calcd for $C_{16}H_{38}ClN_2P_4Ta$ (**7**): C, 32.09; H, 6.40; N, 4.68; P, 20.69. Found: C, 32.29; H, 6.15; N, 4.37; P, 19.97.

Reduction of [NbCl$_4$(dmpe)$_2$] in the Presence of CO and CNBu^t. To a solution of 0.150 g (0.280 mmol) of [NbCl$_4$(dmpe)$_2$] in 20 mL of THF was added 1.5 equiv (0.421 mmol) of Mg (catalytic anthracene). The blue mixture slowly turned green over a 5-min period. At this time, 1 equiv each of CNBu^t (32 μL) and CO (6.8 mL) was coinjected into the reaction vessel. After 25 min the solution was deep burgundy. The reaction was worked up as above for **7** yielding an orange-red solid. Spectroscopic examination indicated the presence of roughly equivalent amounts of [Nb(CNBu^t)(CO)(dmpe)$_2$Cl] (**2**) and a second species, identified as [Nb(CNBu^t)$_2$(dmpe)$_2$Cl] on the basis of IR and NMR spectra that were similar to those of **7**. Attempts to separate the two species were unsuccessful.

Collection and Reduction of X-ray Data. General Procedures. Single-crystal X-ray diffraction studies were carried out on an Enraf-Nonius CAD-4F κ geometry diffractometer employing graphite-monochromated Mo K$\bar{\alpha}$ radiation ($\bar{\lambda}$ = 0.710 73 Å). The diffractometer was configured with a crystal-to-detector distance of 173 mm and a takeoff angle of 2.90°. For room-temperature experiments, crystals were mounted with silicone grease in Lindemann glass capillaries in a nitrogen-filled glovebox. Crystals studied at low-temperature were initially deposited on a mounting stage and bathed with a cold nitrogen stream. The crystal chosen for X-ray analysis was then mounted on the end of a quartz fiber with silicone grease and transferred rapidly to the goniometer. Cooling for the remainder of the low-temperature studies was provided by an Enraf-Nonius FR558-S nitrogen cryostat, calibrated with a copper–constantan thermocouple. After crystals were carefully centered optically in the X-ray beam, an automatic search routine was used to locate up to 25 reflections, which were used to calculate a preliminary unit cell. After

analysis of the initial unit cell for higher symmetry and centering,[41] the cell parameters were refined on the basis of up to 25 carefully measured reflections with $2\theta > 18°$. In each case, the crystal quality and the unit cell choice were checked by examination of axial photographs and several open-counter ω-scans for low-angle reflections.

[Nb(CNCy)(CO)(dmpe)$_2$Cl] (3). Crystals of **3** were grown by slow cooling of a concentrated pentane solution to −30 °C. A plate bound by the faces (100), (010), (001), ($\bar{1}$00), (0$\bar{1}$0), and (00$\bar{1}$) and measuring 0.08 × 0.20 × 0.36 mm was mounted at low temperature as described above. The ω-scans exhibited a mean average peak width at half-height of 0.26°, indicating good crystal quality. The crystal was found to have $2/m$ Laue symmetry and systematic absences consistent with space group $P2_1/a$ (C_{2h}^5, No. 14, cell choice 3),[42] the space group in which data were collected. Data were later transformed to $P2_1/c$ for solution and refinement of the structure.

Intensity data were collected by using an $\omega/2\theta$ scan technique with a variable scan width, $\Delta\omega = (0.62 \pm 0.35 \tan\theta)°$. Backgrounds were measured by extending the calculated width on either end of the scan by 25%. A fixed vertical detector aperture (4 mm) and a variable horizontal detector aperture ($3 + \tan\theta$ mm) were employed. Reflections with $I/\sigma(I) < 2$ for the prescan were rejected as weak. In cases where $I/\sigma(I) > 8$, the prescan was accepted as the final measurement of the reflection. Reflections not falling into these two categories were rescanned at speeds down to 0.63° min^{-1} in an attempt to increase $I/\sigma(I)$ to 8. Three intensity standard reflections were measured after every 3600 s of X-ray exposure time in order to monitor crystal decay. Measurement of three orientation standards after every 250 data points allowed for a check of crystal alignment.

The intensity (I) and the standard deviation [$\sigma(I)$] for each reflection were calculated with eqs 4 and 5, respectively, where C is the total number

$$I = S(C - 2B) \tag{4}$$

$$\sigma(I) = S(C + 4B)^{1/2} \tag{5}$$

of integrated counts, B is the sum of the left and right backgrounds, and S is the scan rate. Observed structure factors and their standard deviations were calculated by using eqs 6 and 7, where A is an attenuator factor (set

$$F_o = (AI/LpTD)^{1/2} \tag{6}$$

$$\sigma(F_o) = [A^2S^2(C + 4B) + (pI)^2]^{1/2}/(2F_oLpTD) \tag{7}$$

to 1.0 if no attenuation was necessary), Lp is a term to correct for Lorentz and polarization effects, T is a transmission factor, and D is a decay correction factor. The pI term, with p set to 0.05, served to avoid overweighting the most intense reflections. No crystal decay was noted for **3**, so D was set as 1.0 for all reflections. Transmission factors were calculated by an analytical absorption correction routine.[43] See Table I for further details.

[Ta(CNEt)(CO)(dmpe)$_2$Cl] (5). A single, red crystal of **5** bound by the faces (100), (010), (001), ($\bar{1}$00), (0$\bar{1}$0), and (00$\bar{1}$) and measuring 0.23 × 0.18 × 0.06 mm was mounted at low temperature as described above. The crystal was judged to be of acceptable quality on the basis of open-counter ω-scans of several low-angle reflections ($\Delta\bar{\omega}_{1/2} = 0.25$ with no fine structure) and axial photographs. Study on the diffractometer indicated Laue symmetry $2/m$ for the crystal, and the systematic absences were found to be consistent with space group $P2_1/n$ (C_{2h}^5, No. 14, cell choice 2).[42] Data were collected and reduced in a fashion similar to that for **3**; further details are given in Table I.

[Ta(CNBu^t)(CO)(dmpe)$_2$Cl] (6). A small irregularly-shaped plate of **6** measuring 0.08 × 0.12 × 0.25 mm was mounted in a capillary under nitrogen as described above. Open-counter ω-scans ($\Delta\bar{\omega}_{1/2} = 0.31$ with no fine structure) and axial photographs indicated the crystal was of acceptable quality for further study. Data were collected and reduced as described above for **3** and in Table I except that, owing to the long b axis, ω scans were employed. Transmission factors were calculated on the basis of empirical ψ-scan data.[44]

[Ta(CNMe)$_2$(dmpe)$_2$Cl] (7). An irregularly-shaped plate measuring 0.30 × 0.25 × 0.10 mm was mounted on a fiber at low temperature as described above. The crystal was judged acceptable on the basis of open-counter ω-scans ($\Delta\bar{\omega}_{1/2} = 0.34$ with no fine structure) and axial photographs. Study on the diffractometer revealed $\bar{1}$ Laue symmetry, and data were collected as described above for **3** (see Table I for details).

[Nb(CNBu^t)(CO)(dmpe)$_2$Cl] (2). Details of the collection and reduction of data for this compound are supplied as supplementary material. The results are nearly identical to those found independently.[35]

Structure Solution and Refinement. All computations were carried out on either a DEC VAXstation II or a DEC VAXstation 3100. Calculations were performed with the TEXSAN crystallographic software package.[45]

[Nb(CNCy)(CO)(dmpe)$_2$Cl] (3). The niobium atom was located by direct methods and all other non-hydrogen atoms by a series of difference Fourier maps and least squares refinements. The function minimized during refinement is given in eq 8 with the weighting function as described

$$\Sigma w(|F_o| - |F_c|)^2 \tag{8}$$

$$w = 1/\sigma^2(F_o) \tag{9}$$

in eqs 7 and 9. Hydrogen atoms were generated and fixed to "ride" on the attached carbon atom at a distance of 0.95 Å with B_{iso} = 1.2B_{iso}(carbon). Final refinement yielded the residuals given in Table I. The largest ratio of parameter shift to estimated standard deviation in the final cycle of refinement was found to be 0.01. The largest residual electron density found from the difference Fourier map was 0.48 e Å^{-3}, located near the niobium atom. Final atomic positional and equivalent isotropic thermal parameters for non-hydrogen atoms are given in Table II. Anisotropic temperature parameters and positional and thermal parameters for hydrogen atoms are provided as supplementary material.

[Ta(CNEt)(CO)(dmpe)$_2$Cl] (5). The tantalum atom was located by a Patterson synthesis, and all other non-hydrogen atoms were located by

Table II. Final Non-Hydrogen Atom Positional[a] and Equivalent Thermal[b] Parameters for [Nb(CNCy)(CO)(dmpe)$_2$Cl] (3)

atom	x	y	z	B(eq) (Å^2)
Nb	0.21179 (2)	0.00154 (6)	0.18616 (2)	1.97 (2)
Cl	0.14285 (8)	0.1747 (2)	0.2780 (1)	3.88 (7)
P(1)	0.23860 (8)	−0.1297 (2)	0.32188 (8)	2.65 (6)
P(2)	0.10537 (8)	−0.1743 (2)	0.1993 (1)	3.08 (7)
P(3)	0.28699 (8)	0.2337 (2)	0.1818 (1)	3.67 (7)
P(4)	0.15195 (9)	0.1550 (2)	0.0667 (1)	3.72 (7)
O	0.2361 (3)	−0.2154 (6)	0.0419 (3)	5.9 (3)
N	0.3745 (3)	−0.1130 (6)	0.1915 (3)	4.2 (3)
C(1)	0.2260 (3)	−0.1332 (7)	0.0946 (3)	3.5 (3)
C(2)	0.3135 (3)	−0.0705 (7)	0.1885 (3)	2.9 (3)
C(3)	0.4060 (3)	−0.2231 (8)	0.1396 (4)	4.0 (3)
C(4)	0.4266 (3)	−0.1475 (8)	0.0640 (4)	4.4 (3)
C(5)	0.4642 (3)	−0.2519 (9)	0.0099 (4)	4.7 (3)
C(6)	0.5288 (3)	−0.3195 (8)	0.0570 (4)	4.7 (3)
C(7)	0.5093 (3)	−0.3915 (8)	0.1337 (4)	4.7 (3)
C(8)	0.4717 (3)	−0.2866 (8)	0.1855 (4)	4.6 (3)
C(11)	0.1554 (3)	−0.1900 (8)	0.3607 (4)	4.5 (3)
C(12)	0.2818 (3)	−0.0229 (8)	0.4042 (3)	4.1 (3)
C(13)	0.2910 (4)	−0.2954 (8)	0.3298 (4)	5.0 (3)
C(21)	0.1139 (4)	−0.2778 (9)	0.2943 (4)	5.5 (4)
C(22)	0.0190 (3)	−0.0879 (8)	0.2049 (5)	5.4 (4)
C(23)	0.0823 (4)	−0.3137 (8)	0.1242 (5)	5.4 (4)
C(31)	0.2343 (4)	0.3803 (8)	0.1302 (5)	5.9 (4)
C(32)	0.3180 (4)	0.3142 (8)	0.2781 (5)	5.6 (4)
C(33)	0.3679 (4)	0.235 (1)	0.1300 (6)	7.0 (5)
C(41)	0.1996 (4)	0.327 (1)	0.0522 (5)	6.4 (4)
C(42)	0.0623 (4)	0.224 (1)	0.0745 (5)	6.7 (4)
C(43)	0.1429 (5)	0.082 (1)	−0.0345 (4)	7.2 (5)

[a] Numbers in parentheses are estimated standard deviations in the last digit. The atom labeling scheme is given in Figure 3. [b] $B(\text{eq}) = {}^4/_3[a^2\beta_{11} + b^2\beta_{22} + c^2\beta_{33} + \{2ab\cos\gamma\}\beta_{12} + \{2ac\cos\beta\}\beta_{13} + \{2bc\cos\alpha\}\beta_{23}]$.

(41) Lawton, S. L. *TRACER II, A FORTRAN Lattice Transformation-Cell Reduction Program*; Mobil Oil Corp.: Paulsboro, NJ, 1967.
(42) *International Tables for Crystallography*; Hahn, T., Ed.; Kluwer Academic: Dordrecht, 1989; Vol. A, pp 174, 182, 104.
(43) Meulenaer, J. D.; Tompa, H. *Acta Crystallogr.* **1965**, *19*, 1014.
(44) North, A. C. T.; Phillips, D. C.; Mathews, F. S. *Acta Crystallogr.* **1968**, *A24*, 351.
(45) *TEXSAN: Single Crystal Structure Analysis Software*, V. 5.0; Molecular Structure Corp.: The Woodlands, TX, 1989.

Table III. Final Non-Hydrogen Atom Positional[a] and Equivalent Thermal[b] Parameters for [Ta(CNEt)(CO)(dmpe)$_2$Cl] (**5**)

atom	x	y	z	B(eq) (Å^2)
Ta	−0.07144 (3)	0.126585 (9)	0.08000 (3)	1.63 (1)
Cl	−0.2931 (2)	0.18138 (7)	−0.0388 (2)	2.97 (8)
P(1)	−0.2993 (2)	0.08859 (7)	0.1423 (2)	2.43 (8)
P(2)	−0.1937 (3)	0.07783 (8)	−0.1507 (2)	3.10 (9)
P(3)	0.0249 (2)	0.19335 (6)	0.2461 (2)	2.28 (8)
P(4)	0.0811 (2)	0.17331 (6)	−0.0657 (2)	2.14 (7)
O	0.2057 (8)	0.0622 (2)	0.086 (1)	5.0 (3)
N	0.0482 (9)	0.0920 (3)	0.4242 (8)	3.8 (3)
C(1)	0.102 (1)	0.0863 (2)	0.085 (1)	2.8 (3)
C(2)	0.0055 (9)	0.1045 (2)	0.294 (1)	2.6 (3)
C(3)	0.159 (1)	0.0594 (3)	0.500 (1)	4.3 (4)
C(4)	0.310 (1)	0.0626 (5)	0.473 (2)	9.5 (9)
C(11)	−0.4361 (9)	0.0688 (3)	−0.031 (1)	3.0 (3)
C(12)	−0.418 (1)	0.1221 (3)	0.229 (1)	3.6 (4)
C(13)	−0.271 (1)	0.0400 (3)	0.260 (1)	4.4 (4)
C(21)	−0.350 (1)	0.0428 (3)	−0.123 (1)	3.7 (4)
C(22)	−0.282 (1)	0.1052 (4)	−0.328 (1)	5.9 (5)
C(23)	−0.077 (1)	0.0369 (4)	−0.211 (1)	5.8 (6)
C(31)	0.080 (1)	0.2379 (2)	0.140 (1)	3.1 (3)
C(32)	−0.108 (1)	0.2200 (3)	0.331 (1)	4.2 (4)
C(33)	0.192 (1)	0.1890 (3)	0.407 (1)	4.1 (4)
C(41)	0.183 (1)	0.2191 (3)	0.050 (1)	4.1 (4)
C(42)	−0.025 (1)	0.2022 (4)	−0.234 (1)	4.6 (5)
C(43)	0.231 (1)	0.1486 (4)	−0.133 (1)	4.3 (4)

[a] Numbers in parentheses are estimated standard deviations in the last digit. The atom labeling scheme is given in Figure 4. [b] $B(\text{eq}) = {}^4/_3[a^2\beta_{11} + b^2\beta_{22} + c^2\beta_{33} + \{2ab\cos\gamma\}\beta_{12} + \{2ac\cos\beta\}\beta_{13} + \{2bc\cos\alpha\}\beta_{23}]$.

Table IV. Final Non-Hydrogen Atom Positional[a] and Equivalent Thermal[b] Parameters for [Ta(CNBu^t)(CO)(dmpe)$_2$Cl] (**6**)

atom	x	y	z	B(eq) (Å^2)
Ta	0.37244 (5)	0.13696 (1)	0.17956 (5)	3.36 (2)
Cl	0.2816 (5)	0.1942 (1)	−0.0160 (4)	6.2 (2)
P(1)	0.5416 (4)	0.1964 (1)	0.2948 (4)	4.4 (1)
P(2)	0.2257 (4)	0.1807 (1)	0.3269 (4)	5.0 (2)
P(3)	0.4744 (5)	0.1092 (1)	−0.0338 (4)	5.6 (2)
P(4)	0.1652 (6)	0.0951 (2)	0.0207 (6)	7.8 (3)
O	0.302 (2)	0.0716 (4)	0.409 (2)	8.9 (8)
N	0.674 (1)	0.0906 (4)	0.337 (1)	5.9 (6)
C(1)	0.330 (2)	0.0960 (5)	0.324 (2)	5.6 (7)
C(2)	0.562 (1)	0.1075 (4)	0.281 (1)	3.9 (5)
C(3)	0.725 (2)	0.0557 (6)	0.435 (2)	6.3 (7)
C(4)	0.886 (3)	0.053 (1)	0.461 (4)	19 (3)
C(5)	0.687 (3)	0.064 (1)	0.580 (2)	12 (2)
C(6)	0.652 (4)	0.0174 (6)	0.369 (2)	12 (2)
C(11)	0.442 (3)	0.2390 (6)	0.358 (3)	9 (1)
C(12)	0.640 (2)	0.2237 (6)	0.183 (2)	8 (1)
C(13)	0.685 (2)	0.1888 (6)	0.453 (2)	8 (1)
C(21)	0.328 (4)	0.229 (1)	0.405 (5)	22 (3)
C(22)	0.167 (4)	0.159 (1)	0.481 (3)	12 (2)
C(23)	0.056 (3)	0.201 (1)	0.237 (2)	14 (2)
C(31)	0.323 (3)	0.0882 (9)	−0.178 (2)	10 (1)
C(32)	0.564 (3)	0.1462 (7)	−0.127 (2)	10 (1)
C(33)	0.595 (3)	0.0649 (7)	−0.014 (2)	10 (1)
C(41)	0.212 (4)	0.071 (1)	−0.137 (3)	17 (3)
C(42)	0.004 (3)	0.121 (1)	−0.062 (4)	18 (2)
C(43)	0.087 (4)	0.052 (1)	0.092 (4)	18 (3)

[a] Numbers in parentheses are estimated standard deviations in the last digit. The atom labeling scheme is given in Figure 4. [b] $B(\text{eq}) = {}^4/_3[a^2\beta_{11} + b^2\beta_{22} + c^2\beta_{33} + \{2ab\cos\gamma\}\beta_{12} + \{2ac\cos\beta\}\beta_{13} + \{2bc\cos\alpha\}\beta_{23}]$.

a series of least squares refinements and difference Fourier techniques. Refinements as described above for **3** yielded the residuals given in Table I. The largest shift/esd in the final cycle of refinement was 0.03, and the largest peak in the final difference map was 0.78 e Å^{-3}, located near the tantalum atom. Final atomic positional and equivalent isotropic thermal parameters for non-hydrogen atoms are given in Table III. Anisotropic temperature factors and positional and thermal parameters for hydrogen atoms are provided as supplemenatry material.

[Ta(CNBu^t)(CO)(dmpe)$_2$Cl] (6). Structure solution and refinement followed the same procedures described for **5**. Final *R* values are given in Table I. Thermal motion resulted in large isotropic temperature factors for many of the dmpe methyl and methylene carbon atoms. Difference maps generated in the plane of the atoms failed to resolve any disorder,

Table V. Final Non-Hydrogen Atom Positional[a] and Equivalent Thermal[b] Parameters for [Ta(CNMe)$_2$(dmpe)$_2$Cl] (**7**)

atom	x	y	z	B(eq) (Å^2)
Ta(1)	0.23065 (2)	0.26873 (2)	0.40839 (3)	1.86 (1)
Ta(2)	0.25839 (2)	0.77461 (2)	0.15442 (3)	2.00 (1)
Cl(1)	0.0901 (1)	0.2769 (1)	0.4718 (2)	3.26 (7)
Cl(2)	0.2496 (1)	0.6295 (1)	0.1988 (3)	3.95 (8)
P(11)	0.2441 (1)	0.4055 (1)	0.3280 (2)	2.39 (6)
P(12)	0.2925 (1)	0.3851 (1)	0.6556 (2)	3.04 (7)
P(13)	0.1261 (1)	0.1404 (1)	0.2205 (2)	2.66 (6)
P(14)	0.1954 (1)	0.1480 (1)	0.5518 (2)	2.92 (7)
P(21)	0.1386 (1)	0.6716 (2)	−0.0543 (3)	4.25 (9)
P(22)	0.1261 (1)	0.7466 (1)	0.2761 (3)	3.29 (7)
P(23)	0.3939 (1)	0.7743 (1)	0.0733 (2)	2.94 (7)
P(24)	0.3639 (1)	0.8250 (1)	0.4054 (2)	2.93 (7)
N(11)	0.4187 (4)	0.2729 (4)	0.4677 (8)	3.3 (2)
N(12)	0.2952 (4)	0.2584 (4)	0.0835 (7)	3.3 (2)
N(21)	0.2837 (4)	0.9698 (4)	0.2566 (8)	3.6 (3)
N(22)	0.2683 (6)	0.8638 (6)	−0.1312 (9)	5.6 (4)
C(11)	0.3483 (4)	0.2721 (4)	0.4435 (8)	2.5 (2)
C(12)	0.2722 (4)	0.2610 (4)	0.2084 (8)	2.4 (2)
C(13)	0.4921 (5)	0.3436 (6)	0.452 (1)	4.1 (3)
C(14)	0.3664 (6)	0.2354 (8)	0.053 (1)	5.6 (4)
C(21)	0.2746 (5)	0.8968 (5)	0.2196 (8)	2.5 (3)
C(22)	0.2623 (6)	0.8302 (6)	−0.023 (1)	3.9 (3)
C(23)	0.3567 (6)	1.0419 (6)	0.234 (1)	5.7 (4)
C(24)	0.228 (1)	0.923 (1)	−0.159 (2)	10.5 (8)
C(111)	0.2545 (6)	0.4884 (5)	0.490 (1)	4.2 (4)
C(112)	0.1570 (5)	0.4039 (6)	0.202 (1)	3.9 (3)
C(113)	0.3324 (5)	0.4576 (5)	0.236 (1)	3.3 (3)
C(121)	0.3193 (7)	0.4886 (5)	0.613 (1)	4.9 (4)
C(122)	0.2264 (6)	0.3897 (6)	0.798 (1)	5.4 (4)
C(123)	0.3871 (7)	0.3957 (8)	0.774 (1)	6.3 (5)
C(131)	0.0617 (5)	0.0649 (5)	0.319 (1)	4.1 (3)
C(132)	0.0495 (5)	0.1586 (6)	0.095 (1)	4.3 (3)
C(133)	0.1593 (5)	0.0710 (5)	0.090 (1)	3.6 (3)
C(141)	0.1195 (6)	0.0483 (5)	0.436 (1)	4.4 (3)
C(142)	0.1474 (6)	0.1595 (6)	0.722 (1)	4.5 (4)
C(143)	0.2784 (6)	0.1154 (6)	0.617 (1)	4.8 (4)
C(211)	0.0463 (5)	0.6164 (6)	0.031 (1)	5.4 (4)
C(212)	0.1517 (7)	0.582 (1)	−0.174 (2)	9.7 (6)
C(213)	0.0914 (7)	0.711 (1)	−0.193 (1)	8.6 (7)
C(221)	0.0293 (5)	0.6834 (7)	0.140 (1)	5.0 (4)
C(222)	0.1151 (7)	0.6881 (9)	0.422 (1)	6.9 (5)
C(223)	0.1011 (7)	0.8352 (7)	0.362 (2)	7.5 (5)
C(231)	0.4660 (5)	0.7721 (6)	0.230 (1)	3.8 (3)
C(232)	0.3895 (6)	0.6853 (6)	−0.070 (1)	4.7 (4)
C(233)	0.4595 (6)	0.8633 (7)	0.001 (1)	5.4 (4)
C(241)	0.4693 (5)	0.8367 (6)	0.367 (1)	3.9 (3)
C(242)	0.3480 (6)	0.7568 (7)	0.540 (1)	4.6 (4)
C(243)	0.3837 (6)	0.9229 (6)	0.533 (1)	4.8 (4)

[a] Numbers in parentheses are estimated standard deviations in the last digit. The atom labeling scheme is given in Figure 6. [b] $B(\text{eq}) = {}^4/_3[a^2\beta_{11} + b^2\beta_{22} + c^2\beta_{33} + \{2ab\cos\gamma\}\beta_{12} + \{2ac\cos\beta\}\beta_{13} + \{2bc\cos\alpha\}\beta_{23}]$.

and the atoms were all refined with anisotropic temperature parameters. The largest shift/esd in the final cycle of refinement was 0.01, and the largest peak in the final difference map was 0.83 e Å^{-3}, located near the tantalum atom. Final positional and thermal parameters are given in Table IV for non-hydrogen atoms. Anisotropic temperature factors and positional and thermal parameters for hydrogen atoms are provided as supplementary material.

[Ta(CNMe)$_2$(dmpe)$_2$Cl] (7). Compound **7** crystallized with two independent molecules in the asymmetric unit. The two tantalum atoms and the inner coordination sphere were located by direct methods. All other non-hydrogen atoms were located by a series of least squares refinements and difference Fourier techniques. Hydrogen atoms were generated and fixed as described above. All non-hydrogen atoms were refined with anisotropic temperature factors. The largest ratio of parameter shift to estimated standard deviation in the final cycle of refinement was found to be 0.01. The largest residual electron density found in the final difference Fourier map was 0.96 e Å^{-3}, located near Ta(1). Final atomic positional and equivalent isotropic thermal parameters for non-hydrogen atoms are given in Table V. Additional information is available as supplementary material.

[Nb(CNBu^t)(CO)(dmpe)$_2$Cl] (2). Details of the solution and refinement of the structure for this compound are supplied as supplementary material.

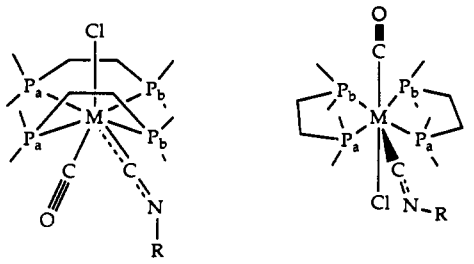

Figure 2. Schematic showing two low-temperature solution structures of compounds **1–6** that are consistent with the NMR data.

Table VI. Infrared Stretching Frequencies (cm^{-1}) for $[ML_2(dmpe)_2Cl]$ Compounds (M = Nb, Ta; L = CO, CNR)[a]

compd	ν(C≡NR)	ν(C≡O)
$[Nb(CO)_2(dmpe)_2Cl]$		1810, 1747
$[Nb(CNMe)(CO)(dmpe)_2Cl]$ (**1**)	1830	1752
$[Nb(CNBu^t)(CO)(dmpe)_2Cl]$ (**2**)	1879 (1840)	1751 (1770)
$[Nb(CNCy)(CO)(dmpe)_2Cl]$ (**3**)	1782	1724
$[Ta(CO)_2(dmpe)_2Cl]$	1810	1740
$[Ta(CNMe)(CO)(dmpe)_2Cl]$ (**4**)	1809	1746
$[Ta(CNEt)(CO)(dmpe)_2Cl]$ (**5**)	1776 (1810)	1722 (1760)
$[Ta(CNBu^t)(CO)(dmpe)_2Cl]$ (**6**)	1808 (1824)	1747 (1760)
$[Ta(CNMe)_2(dmpe)_2Cl]$ (**7**)	1737, 1695	

[a] FTIR spectra recorded from KBr pellets of the listed compounds. Values in parentheses are from solution FTIR spectra recorded in pentane.

Results and Discussion

Synthesis and Spectroscopic Properties of $[M(CNR)(CO)(dmpe)_2Cl]$ Compounds. Photolysis of $[M(CO)_2(dmpe)_2Cl]$ (M = Nb, Ta) complexes in the presence of an excess of an alkyl isocyanide in THF solution resulted in substitution of an isocyanide for one carbonyl ligand (eq 10). The reaction was monitored by

$$[M(CO)_2(dmpe)_2Cl] + RNC \xrightarrow[THF]{h\nu} [M(CNR)(CO)(dmpe)_2Cl] \quad (10)$$

M = Nb, R = Me (**1**), Bu^t (**2**), Cy (**3**)

M = Ta, R = Me (**4**), Et (**5**), Bu^t (**6**)

a darkening of the solution from a yellow-orange to dark red color. The products were easily separated from the starting materials by pentane extraction. This workup resulted in samples pure enough for most uses. In some instances there were small quantities of the starting dicarbonyl complex, which could be removed by recrystallization for all except compound **4**. This complex crystallized with a ~6% dicarbonyl impurity, as judged by $^{31}P\{^1H\}$ NMR at –60 °C, which could not be removed. Yields for the reactions ranged from low (30%) to moderate (65%), depending on the metal and the isocyanide. The lower yields were the result of short photolysis times, necessary because the products themselves are photosensitive. Most of the remaining metal-containing component of the reaction mixture was starting material, which was recovered and purified by chromatography. Longer photolysis times than those reported in the Experimental Section resulted in slightly lower yields and a higher consumption of starting materials.

Other synthetic routes into the mixed isocyanide–carbonyl complexes were investigated. Heating of a THF solution of $[Ta(CO)_2(dmpe)_2Cl]$ and excess *tert*-butyl isocyanide at reflux for 2 days did not result in ligand substitution nor was any reaction observed when a THF solution of $[Ta(CNMe)_2(dmpe)_2Cl]$ (see below) was placed under 8 psig of CO, although decomposition occurred at prolonged reaction times. The addition of 1 equiv each of CO and $CNBu^t$ to a THF solution of $[NbCl_4(dmpe)_2]$ and activated Mg resulted in an inseparable mixture of the bis(isocyanide) and the mixed CO/CNR complex **2**. The photochemical method was therefore judged to be the preferred one for obtaining the desired mixed isocyanide–carbonyl compounds in a pure state.

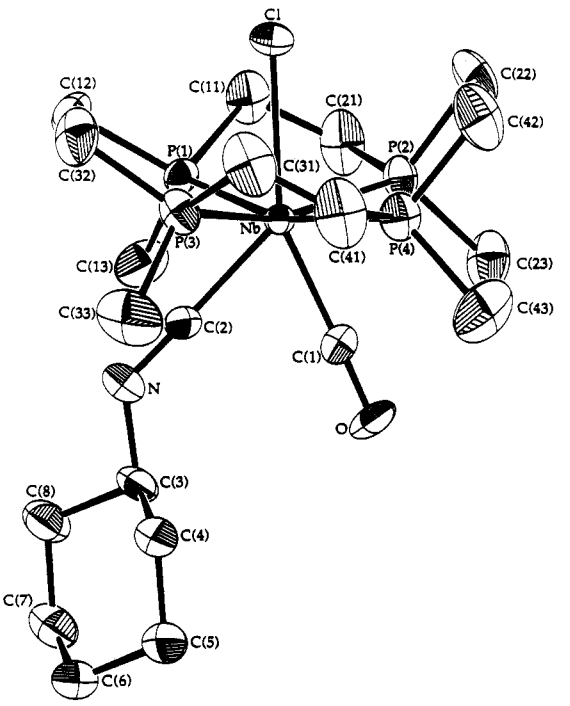

Figure 3. ORTEP diagram of $[Nb(CNCy)(CO)(dmpe)_2Cl]$ (**3**) showing 40% thermal ellipsoids. Hydrogen atoms have been omitted for clarity.

No bis(isocyanide) complexes were detected in the photochemical synthesis of the mixed isocyanide–carbonyl compounds. The complex $[Ta(CNMe)_2(dmpe)_2Cl]$ (**7**) could be prepared, however, by reduction of $[TaCl_4(dmpe)_2]$ in the presence of MeNC, as shown in eq 11. This air-sensitive, dark red solid is extremely soluble in hydrocarbon solvents and was characterized by IR and NMR spectroscopy.

$$[TaCl_4(dmpe)_2] + 2MeNC \xrightarrow[THF]{0.5\%\ Na/Hg} [Ta(CNMe)_2(dmpe)_2Cl] \quad (11)$$
7

As was found for $[M(CO)_2(chelate\ phosphine)_2Cl]$ (M = Nb, Ta) complexes,[46] the isocyanide-substituted species $[M(CNR)_{2-n}(CO)_n(dmpe)_2Cl]$ exhibit fluxional behavior in solution at room temperature on the NMR time scale. All of the mixed isocyanide–carbonyl complexes studied had one or at most two broad ^1H NMR resonances attributed to the methyl groups on the dmpe ligands at room temperature. The $^{31}P\{^1H\}$ NMR spectra of $[Ta(CNR)(CO)(dmpe)_2Cl]$ (R = Me, Et, Bu^t) exhibited only a broad resonance at room temperature. Cooling a THF-d_8 solution of either **4**, **5**, or **6** below –60 °C resolved two sharp doublets in the $^{31}P\{^1H\}$ NMR spectrum, consistent with capped trigonal prismatic or pentagonal bipyramidal geometry (Figure 2).[36] Compound **7** displayed similar fluxional behavior, exhibiting a single signal attributed to the dmpe methyl protons at room temperature, rather than the two expected for a static structure. Fluxional behavior of high-coordinate transition metal complexes in solution is common and has been well studied. The observed averaging of NMR signals for compounds with structures similar to those of **1–7** has been explained by invoking inter-

(46) Brown, L. D.; Datta, S.; Kouba, J. K.; Smith, L. K.; Wreford, S. S. *Inorg. Chem.* **1978**, *17*, 729.

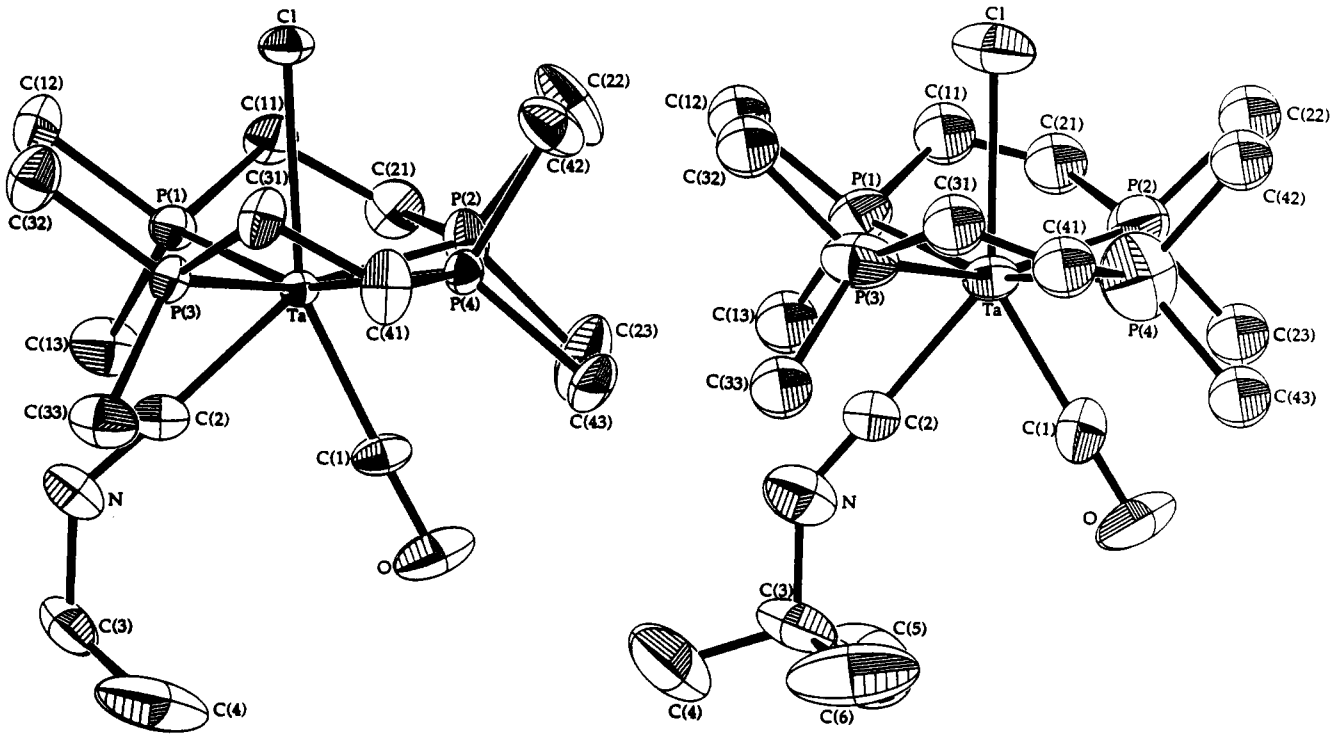

Figure 4. ORTEP view showing the 40% thermal ellipsoids of $[Ta(CNEt)(CO)(dmpe)_2Cl]$ (**5**, left) and $[Ta(CNBu^t)(CO)(dmpe)_2Cl]$ (**6**, right). Hydrogen atoms have been omitted. The dmpe carbon atoms for **6** are shown as spheres with $B = 5$ Å^3 for clarity.

Table VII. Bond Distances (Å) and Angles (deg) for $[Nb(CNCy)(CO)(dmpe)_2Cl]$ (**3**)[a]

	Coordination Sphere Bond Lengths		
Nb–C(1)	2.000 (6)	Nb–P(2)	2.567 (2)
Nb–C(2)	2.030 (6)	Nb–P(3)	2.567 (2)
Nb–Cl	2.633 (2)	Nb–P(4)	2.605 (2)
Nb–P(1)	2.566 (2)		
	Bond Angles		
Cl–Nb–P(1)	80.84 (5)	P(2)–Nb–P(3)	162.03 (6)
Cl–Nb–P(2)	84.09 (5)	P(2)–Nb–P(4)	96.68 (5)
Cl–Nb–P(3)	79.67 (6)	P(2)–Nb–C(1)	80.9 (2)
Cl–Nb–P(4)	85.00 (6)	P(2)–Nb–C(2)	122.3 (2)
Cl–Nb–C(1)	157.6 (2)	P(3)–Nb–P(4)	74.39 (6)
Cl–Nb–C(2)	134.8 (2)	P(3)–Nb–C(1)	112.2 (2)
P(1)–Nb–P(2)	74.04 (5)	P(3)–Nb–C(2)	75.2 (2)
P(1)–Nb–P(3)	110.54 (5)	P(4)–Nb–C(1)	80.4 (2)
P(1)–Nb–P(4)	163.75 (5)	P(4)–Nb–C(2)	122.2 (2)
P(1)–Nb–C(1)	110.5 (2)	C(1)–Nb–C(2)	67.5 (2)
P(1)–Nb–C(2)	73.9 (2)		
	Ligand Geometry Bond Lengths		
C(1)–O	1.186 (7)	N–C(3)	1.489 (8)
C(2)–N	1.213 (7)		
mean P–C	1.824 (7)	range P–C	1.805–1.846
	Bond Angles		
C(2)–N–C(3)	128.6 (5)	N–C(3)–C(4)	108.5 (6)
Nb–C(1)–O	177.8 (5)	N–C(3)–C(8)	108.9 (5)
Nb–C(2)–N	178.7 (5)		
mean C–P–C	101.8 (4)	range C–P–C	100.2–103.7
mean C–C–C	111.0 (6)	range C–C–C	109.4–111.7
mean Nb–P–C	116.4 (3)	range Nb–P–C	110.1–121.3

[a] See Figure 3 for atom labeling scheme. Numbers in parentheses are estimated standard deviations in the last digit(s) given.

Table VIII. Bond Distances (Å) and Angles (deg) for $[Ta(CNEt)(CO)(dmpe)_2Cl]$ (**5**)[a]

	Coordination Sphere Bond Lengths		
Ta–C(1)	1.988 (8)	Ta–P(2)	2.582 (2)
Ta–C(2)	2.019 (9)	Ta–P(3)	2.551 (2)
Ta–Cl	2.616 (2)	Ta–P(4)	2.599 (2)
Ta–P(1)	2.569 (2)		
	Bond Angles		
Cl–Ta–P(1)	78.75 (7)	P(2)–Ta–P(3)	162.17 (7)
Cl–Ta–P(2)	84.96 (8)	P(2)–Ta–P(4)	93.45 (7)
Cl–Ta–P(3)	80.93 (7)	P(2)–Ta–C(1)	80.0 (3)
Cl–Ta–P(4)	83.86 (6)	P(2)–Ta–C(2)	124.7 (2)
Cl–Ta–C(1)	156.9 (3)	P(3)–Ta–P(4)	74.30 (6)
Cl–Ta–C(2)	130.1 (2)	P(3)–Ta–C(1)	109.7 (2)
P(1)–Ta–P(2)	74.48 (7)	P(3)–Ta–C(2)	73.0 (2)
P(1)–Ta–P(3)	113.00 (7)	P(4)–Ta–C(1)	79.7 (2)
P(1)–Ta–P(4)	159.54 (7)	P(4)–Ta–C(2)	126.5 (2)
P(1)–Ta–C(1)	113.5 (2)	C(1)–Ta–C(2)	73.0 (3)
P(1)–Ta–C(2)	73.7 (2)		
	Ligand Geometry Bond Lengths		
C(1)–O	1.19 (1)	N–C(3)	1.45 (1)
C(2)–N	1.22 (1)		
mean P–C	1.82 (1)	range P–C	1.80–1.85
	Bond Angles		
C(2)–N–C(3)	133.1 (9)	Ta–C(2)–N	177.9 (8)
Ta–C(1)–O	178.7 (8)	N–C(3)–C(4)	115.6 (9)
mean C–P–C	101.6 (5)	range C–P–C	100.3–102.7
mean Ta–P–C	116.5 (5)	range Ta–P–C	110.5–120.7

[a] See Figure 4 for atom labeling scheme. Numbers in parentheses are estimated standard deviations in the last digit(s) given.

conversion of capped trigonal prismatic geometries via pentagonal bipyramidal transition states.[46] Such a mechanism would account for the averaging of the phosphine and proton signals on the NMR time scale observed here.

The infrared spectra of **1**–**7** are consistent with their very electron-rich character, as evidenced by the low-energy C≡O and C≡NR stretching frequencies (Table VI). The higher-energy bands are assigned to the isocyanide stretch, because they shift only slightly upon ^{13}C labeling of the carbonyl group, whereas the lower-energy bands shift by ~40 cm^{-1}. Isocyanide IR stretches for neutral complexes are typically in the range 2200–2000 cm^{-1},[47] although in low-valent species they may occur at significantly lower energy. For example, $[Mo(CNMe)_2(dppe)_2]$

(47) Malatesta, L.; Bonati, F. *Isocyanide Complexes of Metals*; Wiley: New York, 1969.

Table IX. Bond Distances (Å) and Angles (deg) for [Ta(CNBu^t)(CO)(dmpe)$_2$Cl] (**6**)[a]

	Coordination Sphere Bond Lengths		
Ta–C(1)	2.00 (2)	Ta–P(2)	2.582 (4)
Ta–C(2)	2.05 (1)	Ta–P(3)	2.574 (4)
Ta–Cl	2.608 (3)	Ta–P(4)	2.554 (5)
Ta–P(1)	2.565 (3)		
	Bond Angles		
Cl–Ta–P(1)	81.0 (1)	P(2)–Ta–P(3)	161.2 (1)
Cl–Ta–P(2)	82.2 (1)	P(2)–Ta–P(4)	99.9 (2)
Cl–Ta–P(3)	79.3 (1)	P(2)–Ta–C(1)	77.3 (5)
Cl–Ta–P(4)	82.8 (2)	P(2)–Ta–C(2)	120.9 (4)
Cl–Ta–C(1)	149.5 (4)	P(3)–Ta–P(4)	74.3 (2)
Cl–Ta–C(2)	139.9 (4)	P(3)–Ta–C(1)	118.0 (5)
P(1)–Ta–P(2)	73.8 (1)	P(3)–Ta–C(2)	76.4 (4)
P(1)–Ta–P(3)	106.5 (1)	P(4)–Ta–C(1)	78.8 (5)
P(1)–Ta–P(4)	163.3 (2)	P(4)–Ta–C(2)	119.7 (4)
P(1)–Ta–C(1)	113.9 (5)	C(1)–Ta–C(2)	70.5 (5)
P(1)–Ta–C(2)	76.0 (4)		
	Ligand Geometry Bond Lengths		
C(1)–O	1.19 (2)	N–C(3)	1.46 (2)
C(2)–N	1.20 (2)		
mean P–C	1.81 (2)	range P–C	1.75–1.88
	Bond Angles		
C(2)–N–C(3)	139 (2)	Ta–C(2)–N	178 (1)
Ta–C(1)–O	179 (1)	N–C(3)–C(4)	108 (2)
mean C–P–C	101 (1)	range C–P–C	97–103
mean Ta–P–C	117 (1)	range Ta–P–C	112–122

[a] See Figure 4 for atom labeling scheme. Numbers in parentheses are estimated standard deviations in the last digit(s) given.

(1886 cm^{-1})[48], [Mo(CNBu^t)$_6$] (1837 cm^{-1})[10], [Fe(CNBu^t)$_5$] (1830 cm^{-1}),[49] and [Fe(PMe$_3$)$_2$(CNMe)$_3$] (1780 cm^{-1})[50] all have isocyanide bands below 1900 cm^{-1}. This shift is caused by the electron-rich metal donating electron density into the C≡NR π^* orbital, formally decreasing the C≡N bond order. In this respect, the isocyanide ligands in compounds **1**–**7** are already activated toward attack by external electrophiles, an important step in the reductive coupling mechanism.[7,10] The carbonyl and isocyanide bands vary considerably depending on the metal and alkyl group (Table VI). These shifts may be caused by solid-state effects, however, since the spectra in solution do not differ nearly as much.

Molecular Structures of [M(CNR)$_{2-n}$(CO)$_n$(dmpe)$_2$Cl] Compounds. Single-crystal X-ray analyses of a representative group of mixed isocyanide–carbonyl compounds revealed very similar structural features. The structure of the niobium(I) compound **3** is shown in Figure 3, and the tantalum(I) complexes **5** and **6** are displayed in Figure 4. A listing of bond distances and angles for **3**, **5**, and **6** are given in Tables VII–IX, respectively, while a comparison of relevant structural features is given in Table X. An X-ray structural study of compound **2** was also undertaken, key geometric features of which are included in Table X. Since the results are in substantial agreement with those recently reported elsewhere,[35] the details of our study are included as supplementary material.

The [M(CNR)(CO)(dmpe)$_2$Cl] complexes adopt a distorted[51] capped trigonal prismatic geometry in the solid state, with which the low-temperature solution NMR data reported above are consistent. The plane of the carbonyl, isocyanide, and chloride ligands roughly bisects the two dmpe ligands, the chelate rings

Table X. Comparison of Selected Bond Distances (Å) and Angles (deg) for [M(CNR)(CO)(dmpe)$_2$Cl][a] (M = Nb, R = Bu^t (**2**); M = Nb, R = Cy (**3**); M = Ta, R = Et (**5**); M = Ta, R = Bu^t (**6**)) Compounds

	2	**3**	**5**	**6**
		Bond Distances		
M–C(1)	1.996 (3)	2.000 (6)	1.988 (8)	2.00 (2)
M–C(2)	2.072 (3)	2.030 (6)	2.019 (9)	2.05 (1)
M–P(1)	2.6030 (8)	2.566 (2)	2.569 (2)	2.565 (3)
M–P(2)	2.5589 (8)	2.604 (2)	2.582 (2)	2.582 (4)
M–P(3)	2.6064 (7)	2.567 (2)	2.551 (2)	2.574 (4)
M–P(4)	2.5653 (7)	2.605 (2)	2.599 (2)	2.554 (5)
M–Cl	2.6362 (7)	2.633 (2)	2.616 (2)	2.608 (3)
O–C(1)	1.179 (3)	1.186 (7)	1.19 (1)	1.19 (2)
N–C(2)	1.193 (3)	1.213 (7)	1.22 (1)	1.20 (2)
N–C(3)	1.456 (3)	1.489 (8)	1.45 (1)	1.48 (3)
		Bond Angles		
M–C(1)–O	179.0 (2)	177.8 (5)	178.7 (8)	179 (1)
M–C(2)–N	177.7 (2)	178.7 (5)	177.9 (8)	178 (1)
C(2)–N–C(3)	144.7 (3)	128.6 (5)	133.1 (9)	139 (2)
C(1)–M–C(2)	67.6 (1)	67.5 (2)	73.0 (3)	70.5 (5)
C(1)–M–P(1)	118.26 (9)	110.5 (2)	113.5 (2)	113.9 (5)
C(1)–M–P(2)	77.61 (9)	80.9 (2)	80.0 (3)	77.3 (5)
C(1)–M–P(3)	116.61 (9)	112.2 (2)	109.7 (2)	118.0 (5)
C(1)–M–P(4)	76.66 (9)	80.4 (2)	79.7 (2)	78.8 (5)
C(1)–M–Cl	141.74 (8)	157.6 (2)	156.9 (3)	149.5 (4)
C(2)–M–P(1)	76.79 (7)	73.9 (2)	73.7 (2)	76.0 (4)
C(2)–M–P(2)	115.30 (7)	122.3 (2)	124.7 (2)	120.9 (4)
C(2)–M–P(3)	77.48 (7)	75.2 (2)	73.0 (2)	76.4 (4)
C(2)–M–P(4)	116.36 (7)	122.2 (2)	126.5 (2)	119.7 (4)
C(2)–M–Cl	150.68 (7)	134.8 (2)	130.1 (2)	139.9 (4)

[a] Numbers in parentheses are errors in the last digit. See Figures 3 and 4 for atom labeling scheme. Bond distances have not been corrected for thermal motion. A complete list of bond distances and angles for compound **2** are available as supplementary material.

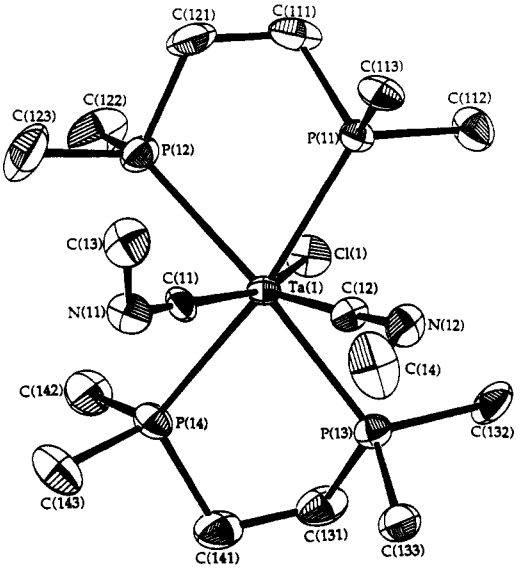

Figure 5. ORTEP diagram showing one molecule of [Ta(CNMe)$_2$(dmpe)$_2$Cl] (**7**) with 40% thermal ellipsoids and omitting hydrogen atoms.

of which are in the asymmetric envelope configuration.[52] For R = Bu^t (**2** and **6**), the bonding of the three non-phosphine ligands is almost symmetric about the metal; that is, the C(1)–M–Cl and C(2)–M–Cl bond angles differ by only ~10°. For R = Et (**5**) and Cy (**3**), however, the structures are distinctly more asymmetric. The isocyanide ligands in these complexes are canted up toward the chlorine atom by ~25° with respect to the carbonyl ligand. This distortion is accompanied by a decrease in the C–N–C bend angles of the isocyanide ligands, 128.6 (5) and 133.1 (9)° for **3** and **5**, respectively, with respect to the values

(48) Chatt, J.; Pombeiro, A. J. L.; Richards, R. L.; Royston, G. H. D.; Muir, K. W.; Walker, R. *J. Chem. Soc., Chem. Commun.* **1975**, 708.
(49) Bassett, J.-M.; Berry, D. E.; Barker, G. K.; Green, M.; Howard, J. A. K.; Stone, F. G. A. *J. Chem. Soc., Dalton Trans.* **1979**, 1003.
(50) Jones, W. D.; Foster, G. P.; Putinas, J. M. *Inorg. Chem.* **1987**, *26*, 2120.
(51) The structures can, alternatively, be described as having distorted C_s 4:3 tetragonal base–trigonal cap piano-stool geometries (see: DeWan, J. C.; Roberts, M. M.; Lippard, S. J. *Inorg. Chem.* **1983**, *22*, 1529).
(52) Hawkins, C. J. *Absolute Configuration of Metal Complexes*; John Wiley & Sons: New York, 1971.

Table XI. Bond Distances (Å) and Angles (deg) for $[Ta(CNMe)_2(dmpe)_2Cl]$ (**7**)[a]

	Coordination Sphere Bond Lengths		
Ta(1)–C(11)	2.022 (7) [2.025 (7)]	Ta(1)–P(12)	2.611 (2) [2.564 (2)]
Ta(1)–C(12)	2.017 (7) [2.018 (8)]	Ta(1)–P(13)	2.551 (2) [2.531 (2)]
Ta(1)–Cl(1)	2.606 (2) [2.591 (2)]	Ta(1)–P(14)	2.589 (2) [2.611 (2)]
Ta(1)–P(11)	2.557 (2) [2.583 (2)]		
	Bond Angles		
Cl(1)–Ta(1)–P(11)	81.10 (6) [77.30 (8)]	P(12)–Ta(1)–P(13)	159.05 (7) [164.64 (8)]
Cl(1)–Ta(1)–P(12)	83.00 (7) [85.27 (7)]	P(12)–Ta(1)–P(14)	93.35 (7) [96.68 (7)]
Cl(1)–Ta(1)–P(13)	78.89 (6) [80.57 (7)]	P(12)–Ta(1)–C(11)	79.3 (2) [84.6 (2)]
Cl(1)–Ta(1)–P(14)	84.68 (6) [81.26 (7)]	P(12)–Ta(1)–C(12)	129.5 (2) [115.9 (3)]
Cl(1)–Ta(1)–C(11)	158.7 (2) [154.7 (2)]	P(13)–Ta(1)–P(14)	74.67 (7) [75.37 (7)]
Cl(1)–Ta(1)–C(12)	129.5 (2) [136.9 (3)]	P(13)–Ta(1)–C(11)	115.8 (2) [105.9 (2)]
P(11)–Ta(1)–P(12)	75.02 (7) [74.82 (8)]	P(13)–Ta(1)–C(12)	71.0 (2) [78.9 (2)]
P(11)–Ta(1)–P(13)	112.06 (7) [107.52 (7)]	P(14)–Ta(1)–C(11)	84.7 (2) [77.0 (2)]
P(11)–Ta(1)–P(14)	162.57 (7) [157.47 (8)]	P(14)–Ta(1)–C(12)	122.9 (2) [128.4 (3)]
P(11)–Ta(1)–C(11)	105.3 (2) [121.8 (2)]	C(11)–Ta(1)–C(12)	71.5 (3) [68.2 (3)]
P(11)–Ta(1)–C(12)	74.3 (2) [73.4 (3)]		
	Ligand Geometry Bond Lengths		
C(11)–N(11)	1.220 (9) [1.210 (9)]	N(11)–C(13)	1.46 (1) [1.50 (1)]
C(12)–N(12)	1.236 (9) [1.23 (1)]	N(12)–C(14)	1.46 (1) [1.48 (1)]
mean P–C	1.83 (1) [1.83 (1)]	range P–C	1.79–1.87
	Bond Angles		
C(11)–N(11)–C(13)	122.1 (7) [124.7 (8)]	Ta(1)–C(12)–N(12)	178.2 (6) [179.1 (7)]
C(12)–N(12)–C(14)	121.8 (7) [124.8 (9)]	Ta(1)–C(11)–N(11)	176.8 (7) [176.9 (8)]
mean C–P–C	101.7 (5) [101.4 (5)]	range C–P–C	99.8–103.5
mean Ta–P–C	116.4 (4) [116.6 (4)]	range Ta–P–C	110.3–121.9

[a] See Figure 5 for atom labeling scheme. Numbers in parentheses are estimated standard deviations in the last digit(s) given. Numbers in square brackets are for the second independent molecule in the unit cell. Note that, in the second molecule, the numbering scheme has been changed such that P(21) corresponds to P(13), P(22) to P(14), P(23) to P(11), P(24) to P(12), etc.

of 144.7 (3) and 139 (2)° found for **2** and **6**. In other respects, the bond distances and angles of the mixed CO/CNR compounds are similar to those found for seven-coordinate dicarbonyl complexes with chelating phosphine ligands.[36]

Isocyanides usually bind to transition metals with nearly linear C–N–C bonds.[47] Strongly π–donating metal fragments, especially low-valent early transition metals with phosphine ligands, may result in a considerable bend in the isocyanide ligand, however.[10,49,50,53-57] This phenomenon is usually attributed to partial metal–isocyanide double bond character inducing sp^2 hybridization at the nitrogen atom, eq 12, although this explanation is

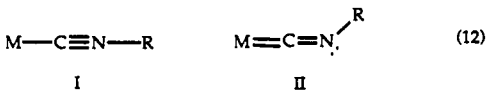

I II (12)

somewhat oversimplified.[13] The presence of good π-accepting ligands, such as carbonyl groups, in the complex tends to decrease the relative π-donation to the isocyanide functionality, resulting in less bending. X-ray structural information and IR spectral data indicate compounds **1–6** already contain significantly reduced isocyanide ligands. Replacement of the remaining CO ligand with a second, more weakly π-accepting isocyanide functionality would be expected to result in a complex containing even more activated isocyanide moieties. To test this idea, a single-crystal X-ray structure determination of the bis(isocyanide) complex **7** was carried out.

An ORTEP diagram of one of the two independent molecules of **7** is shown in Figure 5. A listing of bond distances and angles is given in Table XI. As expected, the isocyanide linkages are extremely bent. In fact, the C(11)–N(11)–C(13) and C(12)–N(12)–C(14) bond angles of 122.1 (7) and 121.8 (7)°, respectively, are far smaller than those determined for the most extensively bent isocyanide ligands previously reported.[10,49,50,53-57] There are many examples of completely linear isocyanides bound to transition metals,[47] but **7** is the first example of an isocyanide complex in which the isocyanide ligands are almost completely stabilized in the heteroallene resonance form II of eq 12. The second molecule of **7** has slightly larger bend angles for the isocyanide ligands, 124.7 (8) and 123.8 (9)°, respectively. Solid-state packing effects and electronic factors both play roles in determining the bend angles of the isocyanide functionalities.

Conclusions

A series of niobium(I) and tantalum(I) mixed isocyanide–carbonyl complexes and the bis(isocyanide) complex $[Ta(CNMe)_2(dmpe)_2Cl]$ have been synthesized and crystallographically characterized. These low-valent complexes are important precursor molecules, based on known criteria[1,4,7,10] for the reductive coupling of CNR with CO or CNR. As reported previously, when $[Nb(CNMe)(CO)(dmpe)_2Cl]$ is subjected to reductive coupling conditions, the new species $[Nb\{Me_3SiOC{\equiv}CN(Me)(SiMe_3)\}(dmpe)_2Cl]$ is generated by reductive coupling of adjacent linear ligands.[33,34] Further details of this interesting chemistry, and that of the bis(isocyanide) compound $[Ta(CNMe)_2(dmpe)_2Cl]$, are available.[34]

Acknowledgment. This work was supported by a grant from the National Science Foundation.

Supplementary Material Available: A textual presentation of the details of the crystal structure determination, tables of crystal data, atomic positional and thermal parameters, and bond distances and angles, and an ORTEP diagram for **2** and tables of anisotropic temperature parameters for the non-hydrogen atoms and positional and thermal parameters for the hydrogen atoms for compounds **3**, **5**, **6**, and **7** (23 pages). Ordering information is given on any current masthead page.

(53) Francis, C. G.; Kahn, S. I.; Morton, P. R. *Inorg. Chem.* **1984**, *23*, 3680.
(54) Chiu, K. W.; Howard, C. G.; Wilkinson, G.; Galas, A. M. R.; Hursthouse, M. B. *Polyhedron* **1982**, *1*, 803.
(55) Green, M.; Howard, J. A. K.; Murray, M.; Spencer, J. L.; Stone, F. G. A. *J. Chem. Soc., Dalton Trans.* **1977**, 1509.
(56) Bassett, J.-M.; Green, M.; Howard, J. A. K.; Stone, F. G. A. *J. Chem. Soc., Chem. Commun.* **1977**, 853.
(57) Barker, G. K.; Galas, A. M. R.; Green, M.; Howard, J. A. K.; Stone, F. G. A.; Turney, T. W.; Welch, A. J.; Woodward, P. *J. Chem. Soc., Chem. Commun.* **1977**, 256.